Clay Minerals UNDEFINED REF -- (2020UNDEFINED REF --), **55**, 329UNDEFINED REF -- –341
doi:10.1180UNDEFINED REF -- /clm.2021.2

CAMBRIDGE UNIVERSITY PRESS

Article

Occurrence of anatase in reworking altered ash beds (K-bentonites and tonsteins) and discrimination of source magmas: a case study of terrestrial Permian–Triassic boundary successions in China

Hanlie Hong[1,2*], Xiaoxue Jin[2], Miao Wan[3], Kaipeng Ji[2], Chen Liu[2], Thomas J. Algeo[1,4,5] and Qian Fang[2]

[1]State Key Laboratory of Biogeology and Environmental Geology, China University of Geosciences, Wuhan, Hubei 430074, China; [2]School of Earth Sciences, China University of Geosciences, Wuhan 430074, China; [3]School of Mathematics and Physics, China University of Geosciences, Wuhan, Hubei 430074, China; [4]State Key Laboratory of Geological Processes and Mineral Resources, China University of Geosciences, Wuhan, Hubei 430074, China and [5]Department of Geology, University of Cincinnati, Cincinnati, OH 45221-0013, USA

Abstract

Potential secondary influences on titanium distribution should be evaluated when using ash beds as volcanic source indicators and for correlation purposes. In this study, well-correlated altered ash beds in Permian–Triassic boundary (PTB) successions of various facies in South China were investigated to better understand their use in source discrimination and stratigraphic correlation. The ash beds deposited in lacustrine and paludal facies contain significantly more Ti relative to deposits in marine facies. Neoformed anatase grains nanometres to micrometres in size are associated closely with clay minerals, whereas detrital anatase was observed in the remnants of altered ash beds of terrestrial facies. Extraction of the clay fraction of altered ash beds may exclude significantly detrital accessory minerals such as anatase and rutile added during sediment reworking, and the concentrations of immobile elements in the clay fraction may therefore be used to interpret more effectively their source igneous rocks.

Keywords: anatase, clay minerals, immobile elements, PTB, titanium, volcanic ash

(Received 18 September 2020; revised 13 January 2021; Accepted Manuscript online: 20 January 2021; Associate Editor: Martine Buatier)

Volcanic ash (<2 mm particle size) from explosive eruptions is often altered into smectite-rich clay rocks (bentonites) during early diagenesis (Christidis & Huff, 2009; Huff, 2016; Hong *et al.*, 2019), after which chemical modification and progressive illitization take place during late diagenesis (Fortey *et al.*, 1996). Altered volcanic ash deposits of marine facies containing mainly mixed-layer illite-smectite (I-S) clays with >3.5% K_2O are usually termed 'K-bentonites' (Merriman & Roberts, 1990; dos Muchangos, 2006), whereas those of non-marine facies containing >50% kaolinite are termed 'tonsteins' (Spears, 2012). In order to avoid inaccurate characterization, we refer to both as 'altered ash beds (or layers)' regardless of their depositional setting (Kiipli *et al.*, 2010). Altered ash layers frequently represent beds corresponding to events that can be correlated in regional chronostratigraphic studies, as they are deposited quickly over wide areas (Huff *et al.*, 1993; Siir *et al.*, 2015; Schindlbeck *et al.*, 2016).

Previous investigations showed that the geochemistry of altered ash beds carries information regarding the type of source magma and the tectonomagmatic setting of the source area, which may be inferred using magmatic and tectonic discriminant diagrams (Huff & Türkmenoğlu, 1981; Ver Straeten, 2004). Alteration of volcanic ash may result in notable changes in the abundances of mobile elements such as K, Na, Ca, Mg and Si (De La Fuente *et al.*, 2000), whereas Al, Ti, high-field-strength elements such as Zr, Nb, Hf and Ta and rare earth elements (*REEs*) are nearly immobile and remain largely unaffected during diagenesis. For this reason, the concentrations and ratios of these elements can be used to draw inferences regarding the source-magma chemistry and tectonic setting of the altered ash beds (Zielinski, 1985; Göncüoğlu *et al.*, 2016). However, the distributions of these so-called immobile elements in ash beds can be affected by depositional and diagenetic processes (*e.g.* through mixing with non-volcanic materials and alteration *via* certain diagenetic pathways; Ver Straeten, 2008). Thus, when using trace elements as source indicators or correlation tools, it is essential to investigate whether the immobile element fraction of volcanic ash has been modified.

Titanium is less mobile during sedimentary and alteration processes than other major elements (Condie *et al.*, 1992), making it useful as an indicator of the provenance of ash beds (Christidis, 1998; Saylor *et al.*, 2005; Batchelor, 2014). However, the mobility of Ti depends on the pH, salinity and redox state of the depositional environment. In particular, extreme pH conditions (*e.g.* high pH in alkaline lakes or low pH in swampy environments due to the decay of organic matter) may facilitate dissolution of Ti-bearing minerals such as anatase and thus loss of Ti from ash beds (McHenry, 2009). Modification of Ti distributions through such processes may make it difficult to accurately identify

UNDEFINED REF -- *Email: 547148099@qq.com

Cite this article: Hong H, Jin X, Wan M, Ji K, Liu C, Algeo TJ, Fang Q (2020). Occurrence of anatase in reworking altered ash beds (K-bentonites and tonsteins) and discrimination of source magmas: a case study of terrestrial PermianUNDEFINED REF -- –Triassic boundary successions in China. *Clay Minerals* **55**, 329UNDEFINED REF -- –341. https://doi.org/10.1180UNDEFINED REF -- /clm.2021.2

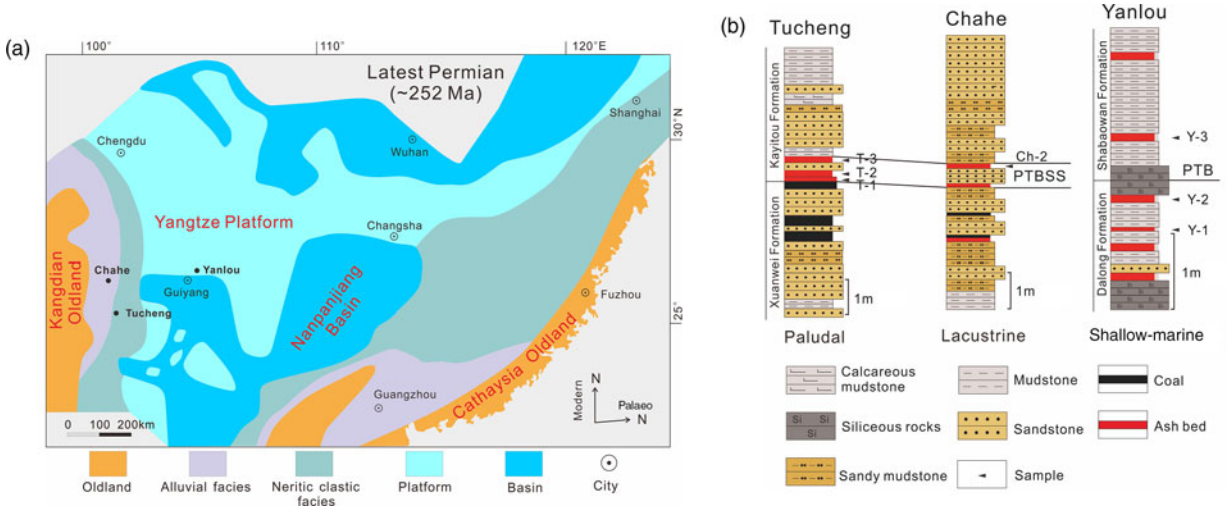

Fig. 1. Study sections and sampling. (a) Palaeogeographical maps of the South China Craton in the latest Permian with section locations; shallow-marine: Yanlou; lacustrine facies: Chahe; paludal facies: Tucheng. (b) Sampling of altered ash beds around the PTB, the stratigraphic position of which is approximate in terrestrial successions, known as the 'Permian–Triassic boundary stratigraphic set' (PTBSS). Modified from Hong *et al.* (2019).

the source-magma type and tectonic setting of an ash bed (Clayton *et al.*, 1996).

In South China, ash deposits occur widely in Permian–Triassic boundary (PTB) successions deposited in various depositional settings. The PTB transition interval commonly contains from one to three ash beds in terrestrial successions and from five to ten ash beds in marine successions, with individual ash beds having thicknesses of 2–40 cm (Yu *et al.*, 2015). The wide occurrence of ash deposits in South China provides an opportunity to investigate the influence of depositional environment on Ti distributions in devitrified ash and the use of ash beds for source-magma discrimination. A recent study showed that marine PTB ash beds experienced no changes in Ti concentrations after deposition, yielding TiO_2/Al_2O_3 ratios similar to those of their intermediate–felsic source magmas, whereas the Ti concentrations of terrestrial facies were commonly modified through reworking and diagenesis (Hong *et al.*, 2019). In the present study, we investigated the distribution of Ti in the extracted clay fractions and remnants of PTB ash samples in two terrestrial sections (Tucheng and Chahe areas) and one shallow-marine section (Yanlou area). The objectives of the present study were to determine the influence of depositional environment on Ti distributions and evaluate the robustness of immobile elements of ash beds as source indicators and correlation tools in various depositional settings.

Geological background

The stratigraphy, mineralogy and geochemistry of ash deposits in many of the PTB successions in South China have been investigated extensively and described in earlier studies (Peng *et al.*, 2005; Yu *et al.*, 2015). Submarine (especially deep-water) weathering of ash materials did not yield any separation of Ti from other immobile elements, and the original distribution of Ti in the altered ash materials remained largely unchanged (Huff *et al.*, 1993; Kiipli *et al.*, 2017). Therefore, the present study was limited to PTB ash beds representing terrestrial (including both paludal and lacustrine) and shallow-marine facies. We collected representative ~500 g ash samples from the ash beds of the three PTB stratigraphic successions.

The Yanlou section (26°32.26? N, 126°60.15? E) is located near Guiyang City, Guizhou Province (Fig. 1). It represents a shallow-marine setting and contains six ash beds with thicknesses ranging from 1 to 10 cm. The ash beds occur within siliceous shale of the Upper Permian Dalong Formation and calcareous mudstone and marl of the Lower Triassic Shabaowan Formation (Hong *et al.*, 2019).

The Tucheng section (25°36.12? N, 104°24.18? E) is located in Panxian County, Guizhou Province, at a distance of ~250 km south-west of the Yanlou section (Fig. 1a). It represents paludal (marine–terrestrial transitional) facies and contains three ash beds with thicknesses ranging from 15 to 40 cm. The ash layers are interbedded with muddy siltstone layers of the Upper Permian Xuanwei Formation and Lower Triassic Kayitou Formation (Peng *et al.*, 2005).

The Chahe section (26°42.08? N, 103°47.36? E) is located between the 31st and 32nd kilometre milestones on the township road between Heishitou and Haila, Weining County, Guizhou Province, at a distance of ~100 km north-west of the Tucheng section (Fig. 1a). It represents fluvial and lacustrine facies that contain two ash beds with thicknesses of 8–10 cm. The ash layers occur in the Upper Permian Xuanwei Formation, in which lacustrine ash beds are interbedded with coal measures, and in the Lower Triassic Kayitou Formation (Yu *et al.*, 2015).

Methods

X-ray diffraction analysis

Whole-rock samples were dried at 60°C overnight and then ground using a mortar and pestle to a ~200 mesh powder that was re-dried at 105°C for 3 h. For clay mineral analysis, the <2 μm clay fraction was extracted using the sedimentation method described by Jackson (1978), leaving a coarser counterpart referred to as the 'remnant'. The extraction procedure is described briefly as follows: a total mass of ~5 g was placed in a 1000 mL beaker and was then mixed with 1000 mL of distilled water and subsequently stirred for 2 h. The suspension was allowed to settle for 6 h and the <2 μm clay fraction was collected by centrifuging the upper clear solution, whereas the remnant

https://doi.org/10.1180/clm.2021.2 Published online by Cambridge University Press

was collected by centrifuging the lower part of the suspension. Both the clay fraction and the remnant were collected for X-ray diffraction (XRD) analysis. Oriented mounts were prepared by carefully pipetting the suspension onto glass slides that were then air-dried at room temperature.

The XRD measurements were performed with a Panalytical X'Pert PRO diffractometer. The instrument was operated at 40 kV and 30 mA, with Ni-filtered Cu-*Kα* radiation with a 1° divergence slit, 1° anti-scatter slit and 0.3 mm receiving slit. The XRD traces were recorded from 3 to 65°2θ at a scan rate of 4°2θ min^{-1} with a resolution of 0.02°2θ.

X-ray fluorescence analysis

Determination of major element compositions was performed for both the clay fractions and remnants using X-ray fluorescence (XRF) (Hong *et al.*, 2017). Briefly, preparation of fused sample pellets entailed: (1) addition of 5 g of dilithium tetraborate to 1 g of sample powder followed by homogenization; (2) addition of four drops of 1.5% LiBr followed by further homogenization; (3) addition of 0.5 mL of polyvinyl alcohol followed by a final homogenization for 10 min; and (4) fusion of this mixture using a hydraulic press and heating with a Philips Perl'X 3 automatic bead machine. Measurements were carried out using a Shimadzu XRF-1800 sequential XRF spectrometer. The relative standard deviations of major elements were generally <1%, and the detection limits of the major elements were ~0.01%. Loss on ignition (LOI) was measured as the difference in sample weight before and after heating at 1000°C. The chemical index of alteration (CIA) of altered ash materials was obtained using the following equation:

$$CIA = Al_2O_3/(Al_2O_3 + CaO^* + K_2O + Na_2O) \times 100\%$$

where CaO^* is the CaO in silicates (Nesbitt & Young, 1982).

Inductively coupled plasma mass spectrometry analysis

The trace element and *REE* concentrations of the clay fractions and remnants were analysed using inductively coupled plasma mass spectrometry (ICP-MS), as described by Hong *et al.* (2017). Briefly, the sample digestion procedure entailed: (1) adding a few drops of ultra-pure water to 50 mg of powdered sample in a Teflon bomb, followed by mixing with 1.5 mL HNO_3 + 1.5 mL HF and heating at 190°C in an electric oven for 48 h; (2) heating the Teflon bomb at 115°C and allowing it to evaporate completely, then adding 1 mL HNO_3 to the dried residue and allowing it to be dissolved and further evaporated completely; (3) adding HNO_3 to dissolve the residue in a Teflon bomb and heating to 190°C for 16 h; and (4) diluting the resulting solution to 100 mL by addition of a 2% HNO_3 solution. Analyses were performed using an Agilent 7500a ICP-MS spectrometer, and the relative standard deviations were usually <10% for trace elements and <4% for *REEs*.

Microscopic observations

The occurrence of anatase in ash samples was observed using scanning electron microscopy (SEM) and high-resolution transmission electron microscopy (HRTEM). A small amount of powdered clay fraction was fixed on a sample holder and then coated with gold. The SEM analysis was performed using a Quanta200 scanning electron microscope equipped with an X-ray energy-dispersive detector. The SEM instrument was operated at an accelerating voltage of 15–20 kV and a beam current of 10–20 nA, with a resolution of 3.5 nm for the secondary electron image. Prior to HRTEM analysis, the powdered clay sample was immersed in methanol solution and dispersed ultrasonically for 15 min. The clay sample was collected using a copper net and then dried under infrared light. The HRTEM analysis was carried out using a JEM 2010FEF transmission electron microscope equipped with an energy dispersive spectrometer (EDS) system at a resolution of 1 Å and an accelerating voltage of 200 kV.

Results

Mineralogical composition of the clay fraction and remnant

The clay fractions and remnants in all samples contain the same assemblage of minerals but in various proportions. In addition, ash samples from different facies yield differing mineral assemblages (Fig. 2). The Tucheng samples consist mainly of kaolinite and mixed-layer kaolinite-smectite (K-S) minerals, with minor quartz, lepidocrocite and anatase. The mixed-layer K-S was identified in previous works (Hong *et al.*, 2017, 2019). The characteristic peaks of kaolinite, lepidocrocite and anatase are markedly stronger, and that of quartz markedly weaker, in the clay fraction compared to the remnants. Furthermore, the peaks of the $(1\bar{1}0)$ diffraction bands of kaolinite are better separated and stronger in the XRD trace of the remnant compared with that of the clay fraction, indicating that the crystal order of kaolinite is higher in the remnant.

The Yanlou and Chahe samples have similar mineral assemblages consisting mainly of mixed-layer I-S minerals and minor quartz and anatase. In addition, sample Y-2 contains minor smectite and kaolinite. All remnants of the ash samples contain relatively large amounts of quartz compared to their clay fractions, as reflected in the greater XRD peak intensity. The consistent presence of anatase in the clay fractions suggests a close association of this mineral with clay minerals.

Microscopic characteristics of clay minerals and anatase in altered ash beds

There are notable differences in the micromorphology of the clay minerals between ash samples from different sedimentary environments. Clay particles of the paludal ash samples displayed mainly poorly developed pseudo-hexagonal kaolinite flakes, with irregular ragged outlines and a chemical composition consisting mainly of Si and Al based on EDS analysis. Small amounts of clay grains showed poorly defined and irregularly curled edges, indicating the possible presence of mixed-layer K-S minerals (Fig. 3a). Anatase grains were not readily identified by SEM due to their small particle size and anhedral morphology, and their recognition depended on EDS surface scanning. These observations yielded only a few small anatase grains (10–50 nm in size) in close association with clay minerals (Fig. 3a).

Owing to their greater thickness, anatase grains usually display a darker background than the surrounding silicate minerals and are thus easily identified using HRTEM, which was further confirmed by EDS analysis. In the clay fraction, anatase was observed as anhedral grains with diameters of 10–50 nm located on the rims of clay particles or closely mixed with clay minerals, whereas the remnant yielded detrital anatase grains with broken outlines and diameters >100 μm (Fig. 3b).

https://doi.org/10.1180/clm.2021.2 Published online by Cambridge University Press

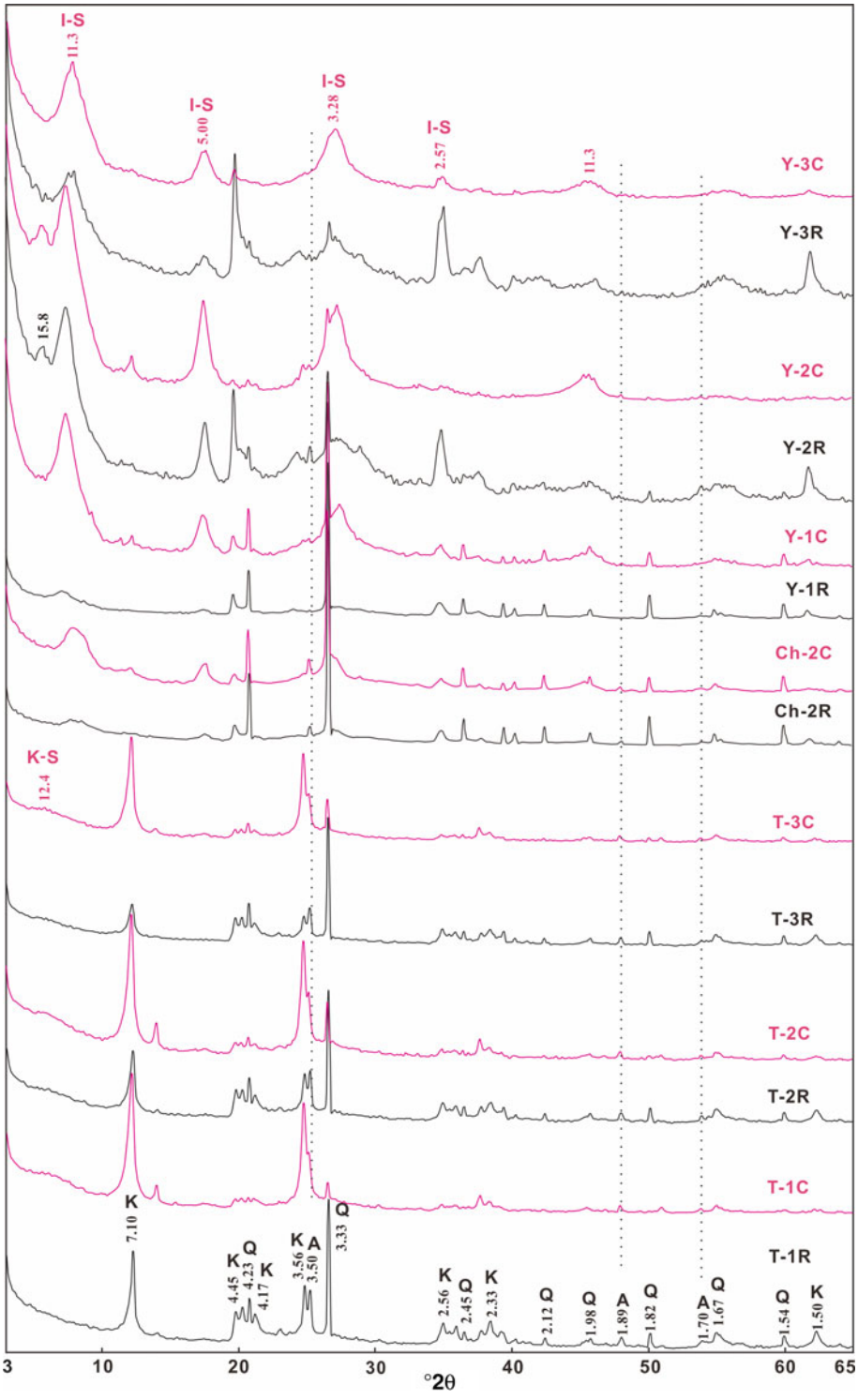

Fig. 2. XRD traces of the clay fraction and remnant. I-S = mixed-layer illite-smectite; K = kaolinite; Q = quartz; F = feldspar; A = anatase; I = illite; T-1C, T-2C, T-3C, Ch-2C, Y-1C, Y-2C, Y-3C = clay fractions of Tucheng, Chahe, and Yanlou sections, and T-1R, T-2R, T-3R, Ch-2R, Y-1R, Y-2R and Y-3R are the remnant counterparts.

Major element compositions of altered ash beds

The major element compositions of the clay fractions and their remnants for ash samples from the different sedimentary facies are given in Table 1. Both the clay fractions and their remnants exhibit rather uniform geochemical compositions with only minor differences within a given sedimentary facies. However, large compositional differences are apparent between the ash beds from paludal facies at Tucheng relative to those of lacustrine facies at Chahe and shallow-marine facies at Yanlou. Paludal ash samples yield LOI values of 13.08–13.80% for the clay fractions and 11.52–11.95% for the remnants, which are notably higher than those for the clay fractions (8.99–11.29%) and remnants (6.44–11.06%) of shallow-marine and lacustrine samples. Paludal ash samples have generally smaller SiO_2 contents for the clay fractions (43.07–45.63%) and remnants (48.67–50.85%) compared to the shallow-marine and lacustrine ash samples (clay: 49.02–54.74%; remnant: 51.01–65.98%). Paludal ash samples

https://doi.org/10.1180/clm.2021.2 Published online by Cambridge University Press

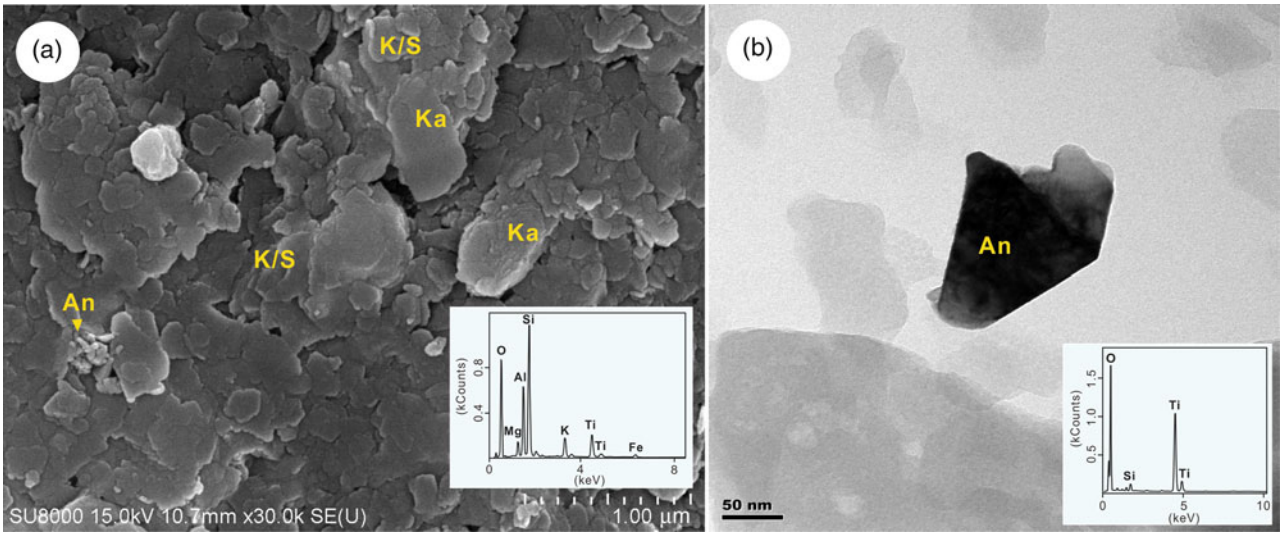

Fig. 3. Microscopic images showing the presence of anatase in altered ash beds. (a) Authigenic anatase in a nano-sized grain adsorbed by clay minerals in Yanlou ash (SEM). (b) Detrital anatase particle in a remnant of Tucheng ash (HRTEM). K-S = mixed-layer kaolinite-smectite; Ka = kaolinite; An = anatase.

exhibit relatively large Al_2O_3 contents (clay: 29.22–30.41%; remnant: 26.47–27.94%) compared to the shallow-marine and lacustrine samples (clay: 21.06–25.29%; remnant: 16.27–25.81%). Paludal ash samples contain markedly more TiO_2 (clay: 3.76–4.03%; remnant: 4.27–4.56%) compared to shallow-marine and lacustrine samples (clay: 0.21–2.03%; remnant: 0.26–1.78%) (Table 1). Paludal ash samples have significantly smaller K_2O contents (clay: 0.90–1.01%, remnant: 0.81–0.91%) than shallow-marine and lacustrine samples (clay: 4.10–4.61%; remnant: 3.39–4.76%). Finally, paludal ash samples contain markedly less MgO (clay: 0.67–0.80%; remnant: 0.51–0.57%) than shallow-marine and lacustrine samples (clay: 1.00–3.24%; remnant: 0.70–3.20%).

Trace element and REE concentrations

The concentrations of trace elements and *REEs* in whole-rock ash samples and their clay fractions are listed in Tables 2 and 3. In general, the upper continental crust-normalized distribution patterns of trace elements of the clay fractions are similar to those of the corresponding whole-rock samples, characterized by notable losses of Cr, Ni, Sr, Ba and Tl (Fig. 4). However, the concentrations of the immobile elements Y and Zr increased slightly, whereas that of Nb decreased in the clay fractions relative to the corresponding whole-rock samples. The lacustrine sample yielded a slightly different pattern: slightly less Y but more Zr and Nb in the clay fraction relative to the whole-rock sample. The concentrations of Y, Zr and Nb are nearly the same in the

TableUNDEFINED REF -- 1. Major chemical compositions of the whole-rock, clay-fraction and remnant samples from the altered ash beds (wt.%).

	Sample	SiO_2	TiO_2	Al_2O_3	Fe_2O_3	MnO	MgO	CaO	Na_2O	K_2O	P_2O_5	LOI	Sum	SiO_2/Al_2O_3	TiO_2/Al_2O_3	CIA	Section	Facies
Whole rock	T-1	48.78	4.85	29.31	3.96	0.01	0.40	0.17	0.00	0.83	0.20	11.89	100.40	2.83	0.21	97.02	Tucheng	Paludal
	T-2	51.18	4.42	26.78	3.87	0.01	0.40	0.07	0.00	0.82	0.16	12.83	100.54	3.25	0.21	96.78	Tucheng	Paludal
	T-3	49.58	4.75	28.85	3.42	0.01	0.43	0.09	0.00	0.84	0.15	12.45	100.57	2.92	0.21	96.94	Tucheng	Paludal
	Ch-2	57.47	2.62	21.61	3.73	0.00	0.79	0.31	0.00	4.45	0.05	9.42	100.45	4.52	0.15	81.74	Chahe	Lacustrine
	Y-1	51.16	0.85	24.97	3.08	0.09	2.83	0.07	0.01	4.45	0.04	12.38	99.93	3.48	0.04	83.70	Yanlou	Shallow water
	Y-2	67.62	0.33	16.59	2.08	0.01	2.21	0.06	0.00	3.56	0.03	7.56	100.05	6.93	0.03	81.11	Yanlou	Shallow water
	Y-3	52.85	0.51	25.81	3.30	0.02	2.48	0.06	0.00	4.81	0.05	10.46	100.35	3.48	0.03	83.18	Yanlou	Shallow water
Clay fraction	T-1C	43.07	3.76	30.41	3.84	0.01	0.72	1.51	0.20	0.90	1.13	13.80	99.34	2.41	0.16	94.90	Tucheng	Paludal
	T-2C	45.09	4.03	29.22	3.88	0.01	0.67	1.33	0.13	0.94	1.11	13.10	99.52	2.62	0.18	95.28	Tucheng	Paludal
	T-3C	45.63	3.77	29.35	3.40	0.01	0.80	1.65	0.18	1.01	1.22	13.08	100.09	2.64	0.16	94.56	Tucheng	Paludal
	Ch-2C	51.70	2.03	23.23	3.03	0.02	1.00	1.61	0.24	4.10	1.09	11.29	99.33	3.78	0.11	81.60	Chahe	Lacustrine
	Y-1C	49.43	0.62	24.46	3.36	0.09	3.23	1.63	0.21	4.58	1.12	10.63	99.35	3.44	0.03	81.21	Yanlou	Shallow water
	Y-2C	54.74	0.41	21.06	3.02	0.02	3.24	1.75	0.20	4.35	1.33	8.99	99.11	4.42	0.02	79.66	Yanlou	Shallow water
	Y-3C	49.02	0.21	25.29	3.15	0.04	2.92	1.88	0.28	4.61	1.56	10.17	99.13	3.30	0.01	81.02	Yanlou	Shallow water
Remnant	T-1R	48.67	4.56	27.94	3.34	0.00	0.51	0.92	0.09	0.81	0.97	11.95	99.77	2.96	0.21	95.96	Tucheng	Paludal
	T-2R	50.07	4.42	27.61	2.76	0.01	0.54	0.91	0.09	0.87	0.83	11.52	99.63	3.08	0.20	95.70	Tucheng	Paludal
	T-3R	50.85	4.27	26.47	3.02	0.00	0.57	0.91	0.08	0.91	0.84	11.65	99.57	3.27	0.21	95.49	Tucheng	Paludal
	Ch-2R	60.51	1.78	17.82	2.34	0.01	0.70	1.17	0.04	3.39	0.66	11.06	99.45	5.77	0.13	82.39	Chahe	Lacustrine
	Y-1R	52.40	0.87	24.53	2.69	0.07	3.20	1.04	0.10	4.71	0.76	9.46	99.83	3.63	0.05	81.85	Yanlou	Shallow water
	Y-2R	65.98	0.34	16.27	2.11	0.01	2.54	0.75	0.21	3.72	0.86	6.44	99.22	6.89	0.03	77.49	Yanlou	Shallow water
	Y-3R	51.01	0.26	25.81	3.05	0.04	2.97	1.31	0.10	4.76	1.33	9.32	99.94	3.36	0.01	82.45	Yanlou	Shallow water

Whole-rock data from Hong *et al.* (2019).

https://doi.org/10.1180/clm.2021.2 Published online by Cambridge University Press

TableUNDEFINED REF -- 2. Concentrations of trace elements and *REEs* of the whole-rock altered ash beds (ppm).

Sample	Li	Be	Sc	V	Cr	Co	Ni	Cu	Zn	Ga	Rb	Sr	Y	Zr	Nb	Sn	Cs	Ba	Ta	Tl	Pb	Th	U
T-1	19.5	3.27	27.1	293	83.4	7.96	58.9	126	45.8	34.8	33.2	272	79.8	555	57.8	5.11	1.97	403	2.87	0.21	29.0	16.9	4.80
T-2	20.4	2.68	26.2	272	75.7	9.08	49.1	123	51.3	34.2	37.0	180	74.2	535	53.3	4.58	1.83	292	3.01	0.13	16.8	16.2	4.69
T-3	17.1	2.67	26.2	270	76.8	7.78	47.2	117	53.3	34.3	37.5	163	70.9	537	56.2	4.76	1.93	297	3.09	0.15	15.5	16.4	4.56
Ch-2	1.62	5.08	32.6	265	214	5.25	28.2	132	27.2	28.8	105	35.5	132	295	31.9	3.00	3.01	108	2.01	0.31	6.28	11.2	3.10
Y-1	58.4	3.89	17.6	78.7	11.6	37.1	21.0	39.4	109	33.6	151	16.2	75.9	408	25.4	8.41	21.2	127	1.99	0.79	42.8	38.8	9.42
Y-2	39.8	1.94	12.9	21.2	11.3	4.61	17.1	56.0	47.8	22.5	130	10.5	64.7	261	19.2	6.64	10.8	56.1	1.47	0.66	10.3	31.2	4.36
Y-3	41.4	3.31	18.6	153	62.9	5.21	12.8	77.5	48.4	28.6	186	63.5	43.1	253	22.9	5.68	14.7	274	1.58	1.50	22.2	23.2	4.54

Sample	La	Ce	Pr	Nd	Sm	Eu	Gd	Tb	Dy	Ho	Er	Tm	Yb	Lu	Hf	ΣREE	ΣLREE	ΣHREE	ΣLREE/ΣHREE	Nb/Y	$Zr/TiO_2 \times 10^{-4}$	δEu
T-1	105	213	30.7	130	26.4	6.74	22.2	3.14	16.8	3.00	7.84	1.10	6.56	0.94	14.4	573	512	61.6	8.31	0.72	0.011	0.83
T-2	101	194	28.5	116	22.4	5.80	18.6	2.67	14.2	2.66	6.92	0.94	5.83	0.85	14.0	520	468	52.7	8.88	0.72	0.012	0.85
T-3	95.7	184	27.3	109	20.8	5.60	17.8	2.55	13.7	2.49	6.60	0.90	5.62	0.80	13.8	493	442	50.5	8.77	0.79	0.011	0.87
Ch-2	222	341	84.4	361	76.7	19.9	63.3	7.85	34.9	5.32	11.6	1.42	7.52	1.04	7.93	1238	1105	133.0	8.31	0.24	0.011	0.85
Y-1	72.8	145	17.0	59.7	12.8	1.59	11.8	2.02	12.0	2.45	7.32	1.07	6.32	0.92	12.0	353	309	43.9	7.04	0.33	0.048	0.39
Y-2	48.9	84.9	11.4	41.7	8.39	1.31	8.14	1.52	10.3	2.23	6.53	0.99	6.12	0.89	7.75	233	197	36.7	5.35	0.30	0.079	0.48
Y-3	67.5	119	14.2	47.1	8.45	1.80	6.87	1.21	7.11	1.42	4.28	0.63	3.86	0.56	7.01	284	258	25.9	9.95	0.53	0.050	0.70
CI chondrite	0.367	0.957	0.137	0.711	0.231	0.087	0.306	0.058	0.381	0.085	0.249	0.036	0.248	0.038								

Carbonaceous Ivuna (CI) chondrite values from Taylor and McLennan (1985); $\delta Eu = Eu_N / ((Sm_N + Gd_N) / 2)$, where Eu_N, Sm_N and Gd_N refer to their chondrite-normalized values.

TableUNDEFINED REF -- 3. Concentrations of trace elements and *REEs* of the clay fractions extracted from the altered ash beds (ppm).

Sample	Li	Be	Sc	V	Cr	Co	Ni	Cu	Zn	Ga	Rb	Sr	Y	Zr	Nb	Sn	Cs	Ba	Ta	Tl	Pb	Th	U
T-1C	16.1	4.11	33.1	309	86.3	9.03	70.5	136	84.4	41.7	36.5	467	102	682	36.8	5.24	2.35	595	2.55	0.21	52.2	16.8	4.57
T-2C	13.1	3.07	30.4	305	80.8	9.32	56.3	148	87.9	38.7	40.5	280	95.0	644	30.9	4.91	2.08	321	2.22	0.15	25.5	16.4	4.81
T-3C	23.6	2.99	34.9	282	79.7	8.62	55.4	128	105	42.0	43.3	212	89.3	656	30.0	4.49	2.35	317	2.14	0.16	21.5	16.7	4.79
Ch-2C	2.33	5.24	25.7	384	278	6.62	35.8	92.4	120	38.1	166	59.2	75.4	421	42.2	4.59	5.59	164	3.03	0.49	10.0	15.5	3.96
Y-1 C	54.7	3.90	14.2	102	20.6	29.8	21.3	57.2	131	32.3	149	35.4	62.4	277	15.7	8.82	27.21	133	1.16	1.07	55.1	40.4	7.24
Y-2C	47.2	2.64	15.8	33.3	19.2	6.09	21.1	75.5	87.3	29.5	177	17.5	58.2	262	19.2	9.51	21.94	76.5	1.57	1.16	16.7	33.5	4.25
Y-3C	41.6	3.50	20.0	167	64.3	6.16	15.0	108	78.1	31.3	190	66.1	42.1	286	20.1	7.02	19.46	211	1.48	2.27	44.3	29.5	5.65

Sample	La	Ce	Pr	Nd	Sm	Eu	Gd	Tb	Dy	Ho	Er	Tm	Yb	Lu	Hf	ΣREE	ΣLREE	ΣHREE	ΣLREE/ΣHREE	Nb/Y	$Zr/TiO_2 \times 10^{-4}$	δEu
T-1C	96.1	240	33.4	156	37.2	9.53	33.4	4.50	22.6	3.89	9.89	1.38	7.94	1.14	18.2	657	572	84.7	6.75	0.36	0.018	0.81
T-2C	95.7	231	31.6	142	31.3	8.05	26.6	3.66	19.0	3.42	8.78	1.25	7.21	1.05	17.4	611	540	71.0	7.60	0.33	0.016	0.83
T-3C	81.7	180	25.0	105	22.2	5.84	19.5	2.92	16.5	3.03	8.34	1.23	7.33	1.12	17.5	480	420	60.0	7.00	0.34	0.017	0.84
Ch-2C	144	314	47.2	194	34.3	8.04	25.8	3.31	17.1	2.87	7.28	1.00	5.70	0.81	11.6	805	742	63.9	11.6	0.56	0.021	0.79
Y-1C	83.3	168	20.1	73.3	13.8	1.75	12.0	1.80	9.94	1.98	5.77	0.82	4.95	0.66	8.57	398	360	37.9	9.50	0.25	0.045	0.41
Y-2C	43.6	82.9	11.0	39.2	7.74	1.22	7.64	1.38	9.18	1.99	6.22	0.95	5.86	0.82	8.35	220	186	34.0	5.45	0.33	0.064	0.48
Y-3C	62.6	122	13.0	40.8	7.64	1.61	6.10	1.11	7.18	1.51	4.65	0.71	4.51	0.62	7.66	274	248	26.4	9.38	0.48	0.014	0.70

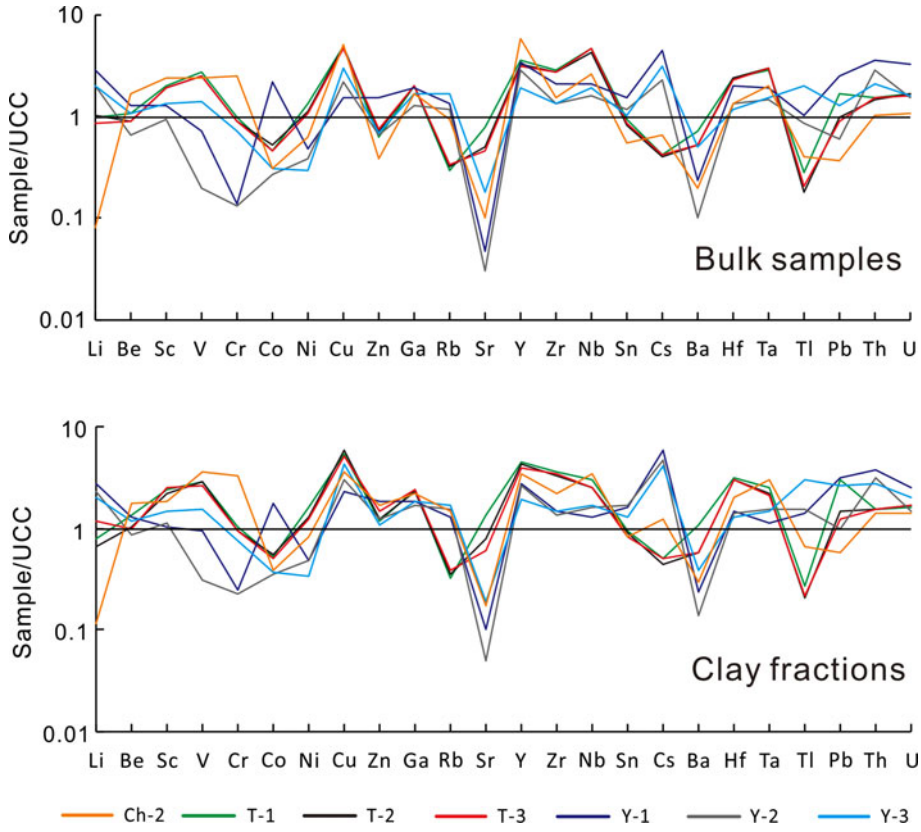

Fig. 4. Trace element distributions of clay fractions and bulk samples of altered ash beds normalized to upper continental crust (UCC; values from Taylor & McLennan, 1985).

clay fractions and whole-rock samples of the shallow-marine samples, except for a slight decrease of Nb in the clay fractions.

The Σ*REE* values of the whole-rock samples from the paludal facies are 573 ppm (T-1), 520 ppm (T-2) and 493 ppm (T-3), which are slightly lower than the values of 657 ppm (T-1), 611 ppm (T-2) and 480 ppm (T-3) of their clay fractions. The Σ*REE* value of 1238 ppm for the lacustrine sample is markedly higher than 805 ppm for its clay fraction. The Σ*REE* values of whole-rock samples of the shallow-marine facies are 353 ppm (Y-1), 233 ppm (Y-2) and 284 ppm (Y-3), which are comparable to those of 398, 220 and 274 ppm, respectively, for their clay fractions.

In general, the bulk altered ash beds and their clay fractions display similar chondrite-normalized *REE* distributions, with only slight differences in abundances (Fig. 5). The *REE* distribution patterns of altered ash beds and clay fractions exhibit a general trend towards enrichment of light *REEs* (*LREEs*) and relatively flat heavy *REE* (*HREE*) patterns, with a moderately negative Eu anomaly. Samples from the shallow-marine facies show a notably larger negative Eu anomaly, with δ_{Eu} values of 0.39–0.70 for bulk ashes and 0.41–0.69 for their clay fractions, whereas samples from the paludal and lacustrine facies show only a small negative Eu anomaly, with δ_{Eu} values of 0.83–0.87 for bulk ashes and 0.79–0.84 for their clay fractions (Table 3). Europium is soluble under strongly reducing diagenetic conditions due to the transformation of Eu^{3+} to soluble Eu^{2+} (Bau, 1991). The larger negative Eu anomaly in shallow-marine ash beds suggests a relatively large loss of Eu in reducing diagenetic environments, whereas the small negative Eu anomaly in paludal and lacustrine ash beds reflects preferential accumulation of Eu under oxidizing diagenetic conditions.

Discussion

Immobile elements during the alteration of ashes

The geochemical characteristics of altered volcanic materials depend largely on the environmental conditions in which the devitrification of volcanic ash takes place (Hong *et al.*, 2019). In closed conditions such as in marine phreatic environments, alteration of volcanic materials does not lead to fractionation of the immobile elements, and consequently their ratios remain unchanged (Bertine, 1974). For this reason, ratios of immobile elements can be used for testing correlations and interpreting source magmas and tectonic environments (Pearce & Peate, 1995; Göncüoğlu *et al.*, 2016). The Nb/Y *vs* Zr/TiO_2 diagram of Winchester and Floyd (1977) is widely used to interpret source magmas of volcanic ash beds (Huff & Türkmenoğlu, 1981; Batchelor & Clarkson, 1993; Kiipli *et al.*, 2017). However, the relative mobility of these elements in altered ash beds during alteration can vary as a function of the depositional environment and the diagenetic pathway (Zielinski, 1985; Clayton *et al.*, 1996; Spears, 2012). In addition, although most altered ash beds are considered as originating from *in situ* weathering of fine-grained, air-fall, pyroclastic volcanic ash, volcanic ashes in lacustrine, paludal and shallow-marine environments are often subject to subaerial erosion, transport and re-deposition of ash, which may result in mixing with terrestrial materials (Naish *et al.*, 1993). These processes may accelerate the dissolution and alteration of volcanic ash and result in the removal of the most mobile components (Christidis, 1998; Arslan *et al.*, 2010). The hydrological setting of an ash deposit influences leaching intensity and transport (*e.g.* with strong leaching and downward flushing in ombrogenous paludal environments; Kiipli *et al.*, 2010; Özdamar *et al.*, 2014). In marine

https://doi.org/10.1180/clm.2021.2 Published online by Cambridge University Press

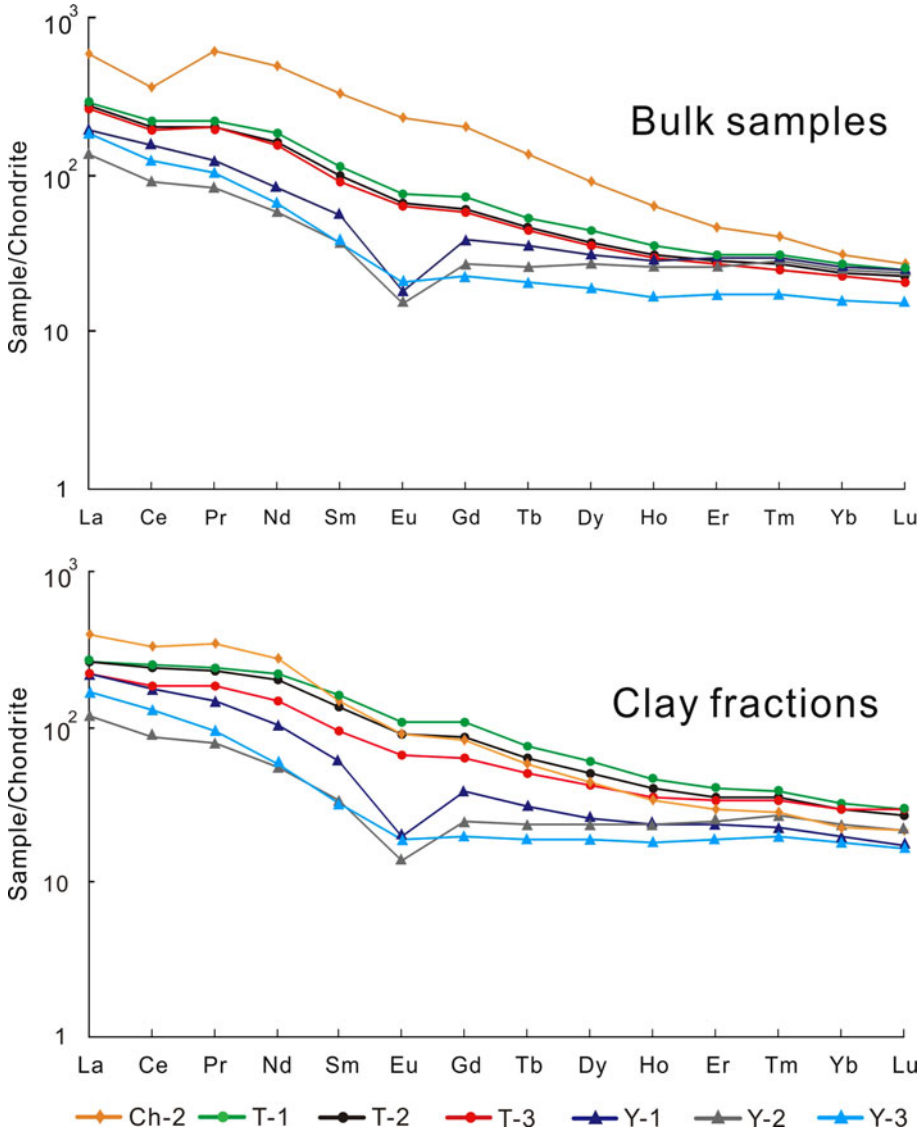

Fig. 5. *REE* distributions of clay fractions and bulk samples of altered ash beds normalized to Carbonaceous Ivuna chondrite compositions (values from Taylor & McLennan, 1985).

environments, ashes are subject to reworking and redistribution by currents, which can change the ratios of immobile elements as the separation of minerals of various densities is closely related to ambient environmental energy (Ver Straeten, 2008).

For ash deposits in open and exoreic lacustrine and paludal environments, immobile element ratios may be modified by weathering, reworking and diagenesis, and careful analysis is required to recognize the post-depositional history of the ash beds (Clayton *et al.*, 1996; Laviano & Mongelli, 1996). In general, the nature of weathering processes and, therefore, the mineralogical and geochemical characteristics of the altered volcanic materials are strongly dependent on depositional facies (Christidis, 1998; McHenry, 2009; Hong *et al.*, 2019). Paludal environments are usually rich in organic acids that promote ash alteration (Zielinski, 1985), leading to intense leaching and the production of mainly kaolinite (Fig. 2). In the present study, paludal ash beds (Tucheng) exhibit intense weathering, as shown by CIA values of 96.78–97.02 and a dominantly kaolinitic mineralogy for whole-rock samples. In contrast, lacustrine (Chahe) and shallow-marine (Yanlou) samples show only intermediate weathering, with CIA values of 81.11–83.70 and a dominance of mixed-layer I-S clays (Fig. 2, Table 1).

All ash samples of a single PTB section tend to display similar *REE* distributions, whereas various patterns are observed for various sections, even within a single depositional facies (Hong *et al.*, 2019). The PTB volcanic ash beds spread through various depositional settings from deep-sea to terrestrial facies within a limited geographical area in western Guizhou, South China. It has been confirmed that the ash beds are the source of intermediate–felsic magmas, deriving from subduction-zone volcanic arcs along the margins of the South China–Indochina and/or South China–Panthalassa plates, which had been active during the Late Permian–Triassic period (Yin *et al.*, 1989; Wu *et al.*, 1990; Stampfli & Borel, 2002; Isozaki *et al.*, 2007; Zhang *et al.*, 2009; Gao *et al.*, 2013; He *et al.*, 2014). The well-correlated PTB volcanic ash beds of various sedimentary facies, with a distance of tens to hundreds of kilometres between different sections in western Guizhou, South China, are reasonably expected to originate from intermediate–felsic rocks. The *REE* distributions of altered ash beds with intermediate–felsic origins usually exhibit a strong negative Eu anomaly (He *et al.*, 2014); therefore, the different *REE* distribution patterns between the ash beds of the different sedimentary facies can probably be attributed to distinct weathering, reworking and diagenesis processes in the geological environments.

https://doi.org/10.1180/clm.2021.2 Published online by Cambridge University Press

In the present study, the paludal samples contain mainly kaolinite and have high *REE* concentrations, and their *REE* distributions, which are characterized by a notably small negative Eu anomaly and right-leaning shape, differ from those of lacustrine and shallow-marine facies (Fig. 5). The lacustrine sample displays similar features to those of the paludal samples, but the former has notably higher Σ*REE* abundances (1105 ppm) compared to the latter (493–573 ppm) (Fig. 5). In general, except for in saline–alkaline conditions, *REEs* tend to be relatively immobile during alteration in most environments (Wood, 1990; Kiipli *et al.*, 2017), and the *REE* distribution patterns of ash beds are largely inherited from the source rocks due to the rapid devitrification of volcanic glass into clay minerals and the sorption processes (Millero, 1992; Arslan *et al.*, 2010; Obst *et al.*, 2015). Thus, ash beds of marine environments exhibit generally the same *REE* distributions as their source materials (Wray, 1995). Compared to the shallow-marine ash beds (Tables 2 & 3), the notably high *REE* abundances and distinctive distribution patterns with a markedly small Eu anomaly of the paludal and lacustrine ashes are probably attributable to concentrations of rare accessory minerals through reworking rather than to elemental mobility during alteration and diagenesis (Zielinski, 1985; Ver Straeten, 2008). This is because in paludal and lacustrine environments, the common anoxic porewaters may cause the reduction and transport of Eu during diagenesis due to their significant sediment organic matter content, leading to a negative Eu anomaly (Bau, 1991). In addition, *REEs* exhibit similar geochemical behaviours in supergene environments and experience negligible fractionation during processes such as weathering, transport and deposition in fine-grained siliciclastic facies (Taylor & McLennan, 1985). In the present study, the paludal ash beds exhibit lamination textures and mixed-layer K-S is present (Hong *et al.*, 2017), observations which confirm that these ash beds experienced subaerial weathering and reworking prior to burial and diagenesis.

Titanium concentrations and source-magma discrimination

In the present study, the whole-rock and clay fractions of a given ash sample generally display similar *REE* distribution patterns and only small differences in Σ*REE*, reflecting a relatively homogeneous distribution of *REEs* (Fig. 5). However, the relative concentrations of the trace elements Nb and Y, as well as those of Zr and TiO_2, show notable differences in the clay fractions of the paludal and lacustrine ash samples, suggesting that these elements are heterogeneously distributed in various grain-size fractions of the sediment. In general, Y tends to be concentrated in the clay fraction relative to Nb (Table 3). Weathering of ash leaches soluble ions from glass phases undergoing dissolution and precipitates clay minerals that can have varying adsorption capacities for certain trace elements, thereby resulting in differential retention patterns among trace elements released from the parent ash (Brookins, 1989; Millero, 1992).

Alteration of volcanic ash involves the devitrification of ash to clay minerals and leaching of alkalis and silica but uptake of Mg, Fe and Ca during the weathering process (Christidis, 1998; Arslan *et al.*, 2010), and the clay species yielded by the ash beds are largely facies-dependent (Hong *et al.*, 2019). Al_2O_3 and TiO_2 are highly immobile chemical components during chemical weathering, and their concentrations will increase with greater degree of weathering due to the net loss of mobile components (Göncüoğlu *et al.*, 2016). Ash beds of the paludal Tucheng section consist mainly of kaolinite and K-S minerals, while those of the shallow-water Yanlou section and the lacustrine Chahe section consist mainly of mixed-layer I-S minerals (Fig. 2). The different clay-mineral assemblages between the PTB sections indicate their various intensities of chemical weathering, which result in the notable differences in Al_2O_3 and TiO_2 concentrations due to the varying degree of leaching of the ash beds (Table 1). Although theoretically the TiO_2/Al_2O_3 ratios of the altered ash beds are inherited from their source magma, the TiO_2/Al_2O_3 values will tend to decrease somewhat as chemical weathering proceeds, as Ti exhibits relatively high mobility in comparison with Al during devitrification of ash to clay minerals (Hodson, 2002; Arslan *et al.*, 2010).

However, in paludal and lacustrine environments, reworking and re-deposition of volcanic ash can potentially lead to an increase in Ti concentration, as an open environment favours the possible migration of very small and light authigenic silicate minerals and the relative accumulation of heavy Ti-bearing phases due to the higher-energy conditions (Ver Straeten, 2004). The paludal and lacustrine ashes are characterized by distinctly higher TiO_2 concentrations (Table 1). Reworking and re-deposition of the volcanic material can lead to mixing with detrital material of terrestrial origin (Clayton *et al.*, 1996; Ver Straeten, 2008). Titanium-bearing accessory minerals such as anatase, rutile, brookite and ilmenite have relatively high densities (4.0–5.0 g cm^{-3}) compared to clay minerals (2.0–2.8 g cm^{-3}) (Berry *et al.*, 1983). As a consequence, reworking and redistribution of volcanic material are liable to mechanical sorting, and these processes can cause significant loss of clay minerals and concurrent enrichment of TiO_2 in the ash bed. In magmas, Ti is generally incorporated in early-crystallized silicate minerals such as biotite, pyroxene and amphibole (Abdel-Rahman, 1994). During devitrification of volcanic ash into clay minerals, Ti is released and forms fine-grained anatase, which usually precipitates in clay-mineral aggregates (Weaver, 1976; Laviano & Mongelli, 1996; Ece & Nakagawa, 2003). Therefore, in marine diagenetic environments, ash-sourced Ti is largely retained in altered ash beds, and no separation of Ti from Al is observed, preserving the initial TiO_2/Al_2O_3 value of the ash bed (Bertine, 1974; Hong *et al.*, 2019).

Organic-rich paludal and lacustrine environments may enhance the mobility of Ti released from primary ash minerals through the formation of $Ti(OH)_4$ colloids (Brookins, 1988; Knauss *et al.*, 2001). However, $Ti(OH)_4$ colloids tend to dehydrate when pH >5 and to precipitate as crystalline TiO_2 (Cornu *et al.*, 1999). As a consequence of this process, Ti-bearing gels often precipitate as an occlusional phase during authigenesis of kaolinite (Malengreau *et al.*, 1995), limiting the range of Ti mobility to short distances (*i.e.* from the nanometre scale to the domain size of detrital Ti-bearing minerals; Tilley & Eggleton, 2005). The paludal and lacustrine ash beds have high TiO_2 contents (2.62–4.85%), and their TiO_2/Al_2O_3 ratios (0.15–0.21; Table 1) are notably higher than the averages for intermediate and felsic source magmas (0.055 and 0.022, respectively) (Le Maitre, 1976). The marked increase in TiO_2 relative to Al_2O_3 probably involves mixing with underlying sediments and mechanical sorting as a consequence of reworking and re-deposition, which would have caused substantial gains of TiO_2 in comparison with Al_2O_3 in the lacustrine and paludal ash beds (Table 1) (Hints *et al.*, 2008; Hong *et al.*, 2019).

The authigenic anatase within an altered ash bed is usually present as nano- to micro-sized grains in close association with

https://doi.org/10.1180/clm.2021.2 Published online by Cambridge University Press

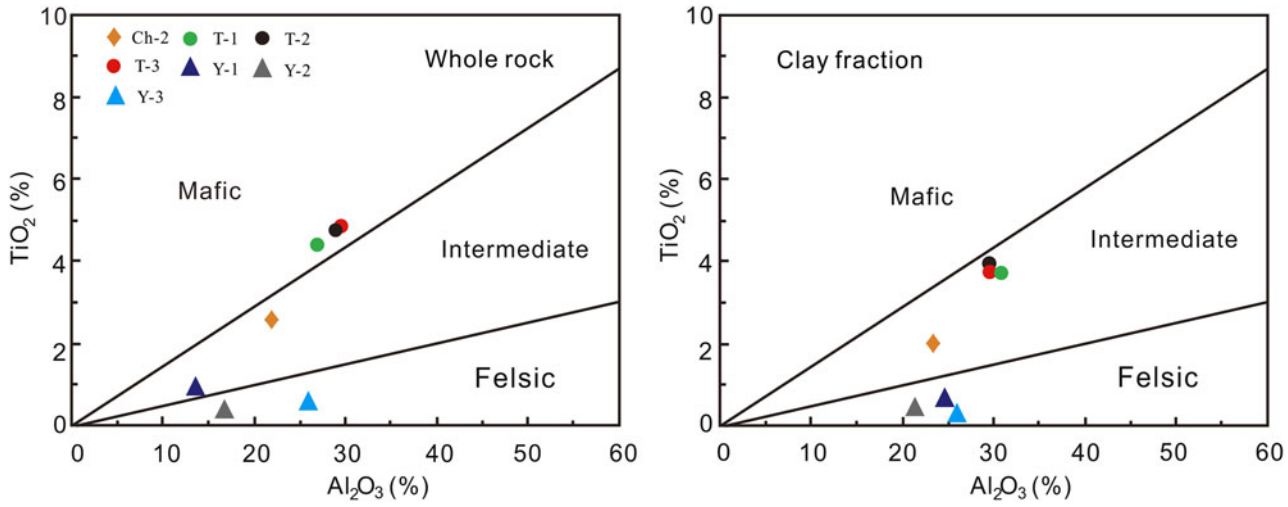

Fig. 6. TiO_2 *vs* Al_2O_3 discrimination plots of the clay fractions and bulk samples of altered ash beds.

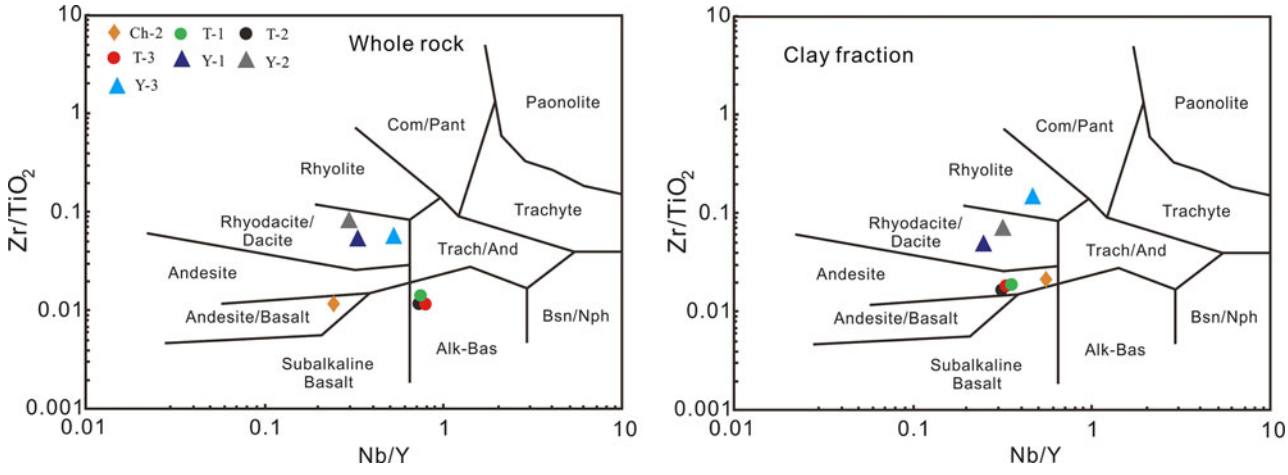

Fig. 7. Zr/TiO_2 *vs* Nb/Y discrimination plots of the clay fractions and bulk samples of altered ash beds. Bsn/Nph = basanite/nephelinite; Alk-Bas = alkaline basalt; Trach/And = trachyte/andesite; Com/Pant = comendite/pantellerite (discrimination diagram after Winchester & Floyd, 1977).

clay minerals (Fig. 3a), whereas Ti-bearing accessory heavy minerals of detrital origin are usually coarse and significantly resistant to alteration. The TiO_2 contents of the clay fractions of the paludal ash samples are mostly lower than those of their remnants (Table 2). The clay fractions consist of kaolinite and mixed-layer K-S, and the remnants mainly of kaolinite (Fig. 2). However, as reflected by the well-separated ($1\bar{1}0$) band peaks, the kaolinite of the remnant fraction is more ordered than that of the clay fraction, consistent with a relatively large particle size. This suggests that Ti-bearing heavy minerals are concentrated in the remnants (Fig. 3b), whereas the clay fraction contains mainly of authigenic anatase grains closely associated with clay minerals (Fig. 3a).

In addition to alteration in diagenesis, the concentration of Ti-bearing heavy minerals in altered ash is also related to the transport of sediments (Schroeder & Shiflet, 2000). The significant TiO_2/Al_2O_3 ratios of lacustrine and paludal ash beds reflect mainly the modification of reworking and diagenesis. As mentioned above, the source magmas of ash beds in the PTB successions of South China contain intermediate–felsic source materials based on the consistent presence of hexagonal dipyramidal quartz, zircon and apatite, as well as the associated sintering glass spherules in the ash beds within PTB successions (Yin *et al.*, 1989; Wu *et al.*, 1990; Zhang *et al.*, 2009; He *et al.*, 2014; Gong *et al.*, 2018). In the present study, the whole-rock samples of the paludal facies plot in the mafic magma field of a TiO_2 *vs* Al_2O_3 discriminant diagram, whereas their clay fractions are projected in the intermediate magma region (Fig. 6). The notable decrease in the TiO_2/Al_2O_3 values of the clay fraction samples is attributable to scavenging of most of the Ti of terrestrial origin through clay-mineral extraction, as neoformed anatase remains in the clay fraction and is associated with clay minerals. Therefore, the Ti content of the clay fraction may serve as a more robust indicator of the source magma of the volcanic ash bed than that of the whole-rock sample (Laviano & Mongelli, 1996). However, during early diagenesis of paludal and lacustrine ashes, the organic-rich environments may enhance the dissolution of Ti from fine-grained detrital Ti-bearing phases due to reworking, and thus increase the uptake of colloidal Ti by clay minerals (Yusoff *et al.*, 2013). Therefore, although clay fractions

https://doi.org/10.1180/clm.2021.2 Published online by Cambridge University Press

may scavenge larger particles of detrital Ti-bearing minerals, the Ti content of the clay fraction can only reduce the influence of detrital Ti-bearing phases in the discrimination of their source rocks. As is shown in Table 1, the clay fractions generally contain less TiO_2 but more Al_2O_3 than the whole-rock samples due to the exclusion of possibly incomplete altering Ti phases of the source material and more enrichment in clay phases; in this case, the clay fractions may provide partial information regarding the geochemical affinities of the parent rocks. Thus, for marine altered ash beds, and especially for deep-water ashes, the immobile chemical components of the whole-rock materials could be used for discrimination of the source magmas (Hong *et al.*, 2019).

The Nb concentrations of the clay fractions are generally lower than those of the whole-rock samples, especially for the paludal ashes (Table 2), mirroring the Ti concentration trends, which is consistent with Nb substituting for Ti in minerals such as ilmenite, rutile, anatase and brookite (Berry *et al.*, 1983). In a Nb/Y *vs* Zr/TiO_2 diagram, the paludal ashes have whole-rock compositions that are projected in the alkaline basalt zone, whereas those of their clay fractions plot in the andesite region (Fig. 7). The clay-fraction results are more robust in that they are consistent with evidence from the associated phenocrysts (Zhang *et al.*, 2009). Mechanical sorting can increase the TiO_2/Al_2O_3 ratio and the Nb/Y value of an ash bed, thereby influencing source-magma inferences based on TiO_2 *vs* Al_2O_3 and Nb/Y *vs* Zr/TiO_2 discriminant diagrams. Thus, for ash beds that have undergone reworking prior to final deposition, which is common for paludal ashes and especially tonsteins (Pearce & Peate, 1995; Spears, 2012), the relative concentrations of immobile elements may differ from those of the original volcanic ash. This can lead to incorrect inferences regarding source magmas based on discriminant diagrams (Clayton *et al.*, 1996). For this reason, we recommend the use of clay-fraction rather than whole-rock immobile element concentrations for source-magma analysis.

Conclusions

Differences in the mineralogical and geochemical characteristics between the clay fractions and remnants of altered ash beds are due to environment-specific differences in weathering and reworking processes. Paludal and lacustrine ash beds are characterized by higher TiO_2 contents, and the presence of detrital Ti-bearing heavy minerals in the remnant is indicative of terrestrial origin. Reworking and re-sedimentation of the original volcanic materials can lead to differential concentrations of the immobile elements, with heterogeneous Nb/Y and Zr/TiO_2 ratios for various grain-size fractions of paludal and lacustrine altered ash beds. Nevertheless, immobile elements are usually retained by clay minerals of the ash beds due to adsorption, and authigenic anatase is present as nano- to micro-sized grains precipitated in clay aggregates. Extraction of the clay fraction from reworked ash beds can exclude detrital heavy minerals, allowing the concentrations of immobile elements in the clay fraction to serve as a more robust proxy for source magmas than those of the whole-rock sample. However, the organic-rich paludal and lacustrine environments may enhance the dissolution of detrital Ti-bearing phases and thus increase the uptake of Ti by clay minerals; therefore, the Ti content of the clay fraction may reduce the influence of detrital Ti-bearing phases in the discrimination of their source rocks owing to scavenging the larger detrital Ti-bearing minerals. By contrast, for marine ash beds, due to the exclusion of the possibly incomplete altering Ti phases of the source magma, Ti of clay fractions may provide partial information regarding the geochemical affinities of the parent rocks; thus, the immobile chemical components of the whole-rock ash beds could be used directly for source discrimination.

Acknowledgements. UNDEFINED REF --   The authors thank Drs J.X. Yu and S.Q. Cao for assistance with sample collection, and Prof G.E. Christidis, Principal Editor, and two anonymous reviewers for their insightful reviews, comments and suggestions.

Financial support. UNDEFINED REF --   This work was supported by the National Natural Science Foundation of China (Projects 41972040 and 41472041) and the Fundamental Research Funds for the Central Universities, China University of Geosciences (Wuhan) (No. CUG170106).

References

Abdel-Rahman A.M. (1994) Nature of biotites from alkaline, calc-alkaline, and peraluminous magmas. *Journal of Petrology*, **35**, 525–541.

Arslan M., Abdìoğlu E. & Kadır S. (2010) Mineralogy, geochemistry, and origin of bentonite in upper cretaceous pyroclastic units of the Tirebolu area, Gìresun, Northeast Turkey. *Clays and Clay Minerals*, **58**, 120–141.

Batchelor R.A. (2014) Metabentonites from the Sandbian Stage (Upper Ordovician) in Scotland – a geochemical comparison with their equivalents in Baltoscandia. *Scottish Journal of Geology*, **50**, 159–163.

Batchelor R.A. & Clarkson E.N.K. (1993) Geochemistry of a Silurian metabentonite and associated apatite from the North Esk Inlier, Pentland Hills. *Scottish Journal of Geology*, **29**, 123–130.

Bau M. (1991) Rare-earth element mobility during hydrothermal and metamorphic fluid-rock interaction and the significance of the oxidation state of europium. *Chemical Geology*, **93**, 219–230.

Berry L.G., Mason B. & Dietrich R.V. (1983) *Mineralogy: Concepts, Descriptions, Determinations*. W. H. Freeman and Company, San Francisco, CA, USA, 561 pp.

Bertine K.K. (1974) Origin of Lau Basin Rise sediment. *Geochimica et Cosmochimica Acta*, **38**, 629–640.

Brookins D.G. (1988) *Eh–pH Diagrams for Geochemistry*. Springer-Verlag, Berlin, Germany, 176 pp.

Brookins D.G. (1989) Aqueous geochemistry of rare earth elements. Pp. 201–225 in: *Geochemistry and Mineralogy of Rare Earth Elements* (B.P. Lipin & G.A. McKay, editors). Reviews in Mineralogy 21. Mineralogical Society of America, Washington, DC, USA.

Christidis G.E. (1998) Comparative study of the mobility of major and trace elements during alteration of an andesite and a rhyolite to bentonite, in the Islands of Milos and Kimolos, Aegean, Greece. *Clays and Clay Minerals*, **46**, 379–399.

Christidis G.E. & Huff W.D. (2009) Geological aspects and genesis of bentonites. *Elements*, **5**, 93–98.

Clayton T., Francis J.E., Hillier S.J., Hodson F., Saunders R.A. & Stone J. (1996) The implications of reworking on the mineralogy and chemistry of lower Carboniferous K-bentonites. *Clay Minerals*, **31**, 377–390.

Condie K.C., Boryta M.D., Liu J. & Quian X. (1992) The origin of khondalites: geochemical evidence from the Archean to Early Proterozoic granulitic belt in the North China Craton. *Precambrian Research*, **59**, 207–223.

Cornu S., Lucas Y., Lebon E., Ambrosi J.P., Luizão F., Rouiller J. *et al.* (1999) Evidence of titanium mobility in soil profiles, Manaus, Central Amazonia. *Geoderma*, **9**, 281–295.

De La Fuente S., Cuadros J., Fiore S. & Linares J. (2000) Electron microscopy study of volcanic tuff alteration to illite-smectite under hydrothermal conditions. *Clays and Clay Minerals*, **48**, 339–350.

dos Muchangos A.C. (2006) The mobility of rare-earth and other elements in the process of alteration of rhyolitic rocks to bentonite (Lebombo Volcanic Mountainous Chain, Mozambique). *Journal of Geochemical Exploration*, **88**, 300–303.

Ece O.I. & Nakagawa Z.-E. (2003) Alteration of volcanic rocks and genesis of kaolin deposits in the Şile Region, northern İstanbul, Turkey. Part II: differential mobility of elements. *Clay Minerals*, **38**, 529–550.

Fortey N.J., Merriman R.J. & Huff W.D. (1996) Silurian and Late-Ordovician K-bentonites as a record of Late Caledonian volcanism in the British Isles. *Transactions of the Royal Society of Edinburgh: Earth Sciences*, **86**, 167–180.

Gao Q.L., Zhang N., Xia W.C., Feng Q.L., Chen Z.Q., Zheng J.P. *et al.* (2013) Origin of volcanic ash beds across the Permian–Triassic boundary, Daxiakou, South China: petrology and U–Pb age, trace elements and Hf-isotope composition of zircon. *Chemical Geology*, **360**, 41–53.

Göncüoğlu M.C., Günal-Türkmenoğlu A., Bozkaya Ö., Ünlüce-Yücel Ö., Okuyucu C. & Yilmaz İ.Ö. (2016) Geological features and geochemical characteristics of late Devonian–early Carboniferous K-bentonites from northwestern Turkey. *Clay Minerals*, **51**, 539–562.

Gong N.N., Huff W.D., Hong H.L., Fang Q., Wang C.W., Yin K. & Chen S.L. (2018) Influences of sedimentary environments and volcanic sources on diagenetic alteration of volcanic tuffs in South China. *Scientific Reports*, **8**, 7616.

He B., Zhong Y.T., Xu Y.G. & Li X.H. (2014) Triggers of Permo-Triassic boundary mass extinction in South China: the Siberian Traps or Paleo-Tethys ignimbrite flare-up? *Lithos*, **204**, 258–267.

Hints R., Kirsimäe K., Somelar P., Kallaste T. & Kiipli T. (2008) Multiphase Silurian bentonites in the Baltic Palaeobasin. *Sedimentary Geology*, **209**, 69–79.

Hodson M.E. (2002) Experimental evidence for mobility of Zr and other trace elements in soils. *Geochimica et Cosmochimica Acta*, **66**, 819–828.

Hong H.L., Algeo T.J., Fang Q., Zhao L.L., Ji K.P., Yin K. *et al.* (2019) Facies dependence of the mineralogy and geochemistry of altered volcanic ash beds: an example from Permian–Triassic transition strata in southwestern China. *Earth-Science Reviews*, **190**, 58–88.

Hong H.L., Fang Q., Wang C.W., Churchman G.J., Zhao L.L., Gong N.N. & Yin K. (2017) Clay mineralogy of altered tephra beds and facies correlation between the Permian–Triassic boundary stratigraphic sets, Guizhou, South China. *Applied Clay Science*, **143**, 10–21.

Huff W.D. (2016) K-bentonites: a review. *American Mineralogist*, **101**, 43–70.

Huff W.D. & Türkmenoğlu A.G. (1981) Chemical characteristics and origin of Ordovician K-bentonites along the Cincinnati Arch. *Clays and Clay Minerals*, **29**, 113–123.

Huff W.D., Merriman R.J., Morgan D.J. & Roberts B. (1993) Distribution and tectonic setting of Ordovician K-bentonites in the United Kingdom. *Geological Magazine*, **130**, 93–100.

Isozaki Y., Shimizu N., Yao J., Ji Z. & Matsuda T. (2007) End-Permian extinction and volcanism-induced environmental stress: the Permian–Triassic boundary interval of lower-slope facies at Chaotian, South China. *Palaeogeography, Palaeoclimatology, Palaeoecology*, **252**, 218–238.

Jackson M.L. (1978) *Soil Chemical Analyses*. Department of Geology, University of Wisconsin–Madison, WI, USA, 498 pp.

Kiipli P., Hints R., Kallaste T., Verš E. & Voolma M. (2017) Immobile and mobile elements during the transition of volcanic ash to bentonite – an example from the Early Palaeozoic sedimentary section of the Baltic Basin. *Sedimentary Geology*, **347**, 148–159.

Kiipli T., Kallaste T. & Nestor V. (2010) Composition and correlation of volcanic ash beds of Silurian age from the eastern Baltic. *Geological Magazine*, **147**, 895–909.

Knauss K.G., Dibley M.J., Bourcier W.L. & Shaw H.F. (2001) Ti(IV) hydrolysis constants derived from rutile solubility measurements made from 100 to 300°C. *Applied Geochemistry*, **16**, 1115–1128.

Laviano R. & Mongelli G. (1996) Geochemistry and mineralogy as indicators of parental affinity for Cenozoic bentonites: a case study from S. Croce Di Magliano (southern Apennines, Italy). *Clay Minerals*, **31**, 391–401.

Le Maitre R.W. (1976) The chemical variability of some common igneous rocks. *Journal of Petrology*, **17**, 589–598.

Malengreau N., Muller J.P. & Calas G. (1995) Spectroscopic approach for investigating the status and mobility of Ti in kaolinitic sediments. *Clays and Clay Minerals*, **43**, 615–621.

McHenry L.J. (2009) Element mobility during zeolitic and argillic alteration of volcanic ash in a closed-basin lacustrine environment: case study Olduvai Gorge, Tanzania. *Chemical Geology*, **265**, 540–552.

Merriman R.J. & Roberts B. (1990) Metabentonites in the Moffat shale Group, Southern uplands of Scotland: geochemical evidence of ensialic marginal basin volcanism. *Geological Magazine*, **127**, 259–271.

Millero F.J. (1992) Stability constants for the formation of rare earth inorganic complexes as a function of ionic strength. *Geochimica et Cosmochimica Acta*, **56**, 3123–3132.

Naish T.R., Nelson C.S. & Hodder A.P.W. (1993) Evolution of Holocene sedimentary bentonite in a shallow-marine embayment, Firth of Thames, New Zealand. *Marine Geology*, **109**, 267–278.

Nesbitt H.W. & Young G.M. (1982) Early Proterozoic climates and plate motions inferred from major element chemistry of lutites. *Nature*, **299**, 715–717.

Obst K., Ansorge J., Matting S. & Huneke H. (2015) Early Eocene volcanic ashes on Greifswalder Oie and their depositional environment, with an overview of coeval ash-bearing deposits in northern Germany and Denmark. *International Journal of Earth Sciences*, **104**, 2179–2212.

Özdamar Ş., Ece Ö.I., Uz B., Boylu F., Ercan H.Ü. & Yanik G. (2014) Element mobility during the formation of the Uzunisa-Ordu bentonite, NE Turkey, and potential applications. *Clay Minerals*, **49**, 609–633.

Pearce J.A. & Peate D.W. (1995) Tectonic implications of the composition of volcanic arc magmas. *Annual Review of Earth and Planetary Sciences*, **23**, 251–285.

Peng Y.Q., Zhang S.X., Yu J.X., Yang F.Q., Gao Y.Q. & Shi G.R. (2005) High-resolution terrestrial Permian–Triassic eventostratigraphic boundary in western Guizhou and eastern Yunnan, southwestern China. *Palaeogeography, Palaeoclimatology, Palaeoecology*, **215**, 285–295.

Saylor B.Z., Poling J.M. & Huff W.D. (2005) Stratigraphic and chemical correlation of volcanic ash beds in the terminal Proterozoic Nama Group, Namibia. *Geological Magazine*, **142**, 519–538.

Schindlbeck J.C., Kutterolf S., Freundt A., Alvarado G.E., Wang K.L., Straub S.M. *et al.* (2016) Late Cenozoic tephrostratigraphy offshore the southern central American Volcanic Arc: 1. Tephra ages and provenance. *Geochemistry, Geophysics, Geosystems*, **17**, 4641–4668.

Schroeder P.A. & Shiflet J. (2000) Ti-bearing phases in the Huber Formation, an East Georgia kaolin deposit. *Clays and Clay Minerals*, **48**, 151–158.

Siir S., Kallaste T., Kiipli T. & Hints R. (2015) Internal stratification of two thick Ordovician bentonites of Estonia: deciphering primary magmatic, sedimentary, environmental and diagenetic signatures. *Estonian Journal of Earth Sciences*, **64**, 140–158.

Spears D.A. (2012) The origin of tonsteins, an overview, and links with seatearths, fireclays and fragmental clay rocks. *International Journal of Coal Geology*, **94**, 22–31.

Stampfli G.M. & Borel G.D. (2002) A plate tectonic model for the Paleozoic and Mesozoic constrained by dynamic plate boundaries and restored synthetic oceanic isochrons. *Earth and Planetary Science Letters*, **196**, 17–33.

Taylor S.R. & McLennan S.M. (1985) *The Continental Crust: Its Composition and Evolution*. Blackwell Science, Cambridge, MA, USA, 312 pp.

Tilley D.B. & Eggleton R.A. (2005) Titanite low-temperature alteration and Ti mobility. *Clays and Clay Minerals*, **53**, 100–107.

Ver Straeten C.A. (2004) K-bentonites, volcanic ash preservation, and implications for Early to Middle Devonian volcanism in the Acadian orogen, eastern North America. *Geological Society of America Bulletin*, **116**, 474–489.

Ver Straeten C.A. (2008) Volcanic tephra bed formation and condensation processes: a review and examination from Devonian stratigraphic sequences. *Journal of Geology*, **116**, 545–557.

Weaver C.E. (1976) The nature of TiO_2 in kaolinite. *Clays and Clay Minerals*, **24**, 215–218.

Winchester J.A. & Floyd P.A. (1977) Geochemical discrimination of different magma series and their differentiation products using immobile elements. *Chemical Geology*, **20**, 325–343.

Wood S.A. (1990) The aqueous geochemistry of the rare-earth elements and yttrium, 1. Review of available low-temperature data for inorganic complexes and the inorganic *REE* speciation of natural waters. *Chemical Geology*, **82**, 159–186.

Wray D.S. (1995) Origin of clay-rich beds in Turonian chalks from Lower Saxony, Germany – a rare earth element study. *Chemical Geology*, **119**, 161–173.

https://doi.org/10.1180/clm.2021.2 Published online by Cambridge University Press

Wu S.B., Ren Y.X. & Bi X.M. (1990) Volcanic material and origin of clay rock near Permo-Triassic boundary from Huangshi, Hubei and Meishan of Changing County, Zhejiang. *Earth Science*, **15**, 589–595 (in Chinese with English abstract).

Yin H.F., Huang S.J., Zhang K.X., Yang F.Q., Ding M.H., Bi X.M. & Zhang S.X. (1989) Volcanism at the Permian–Triassic Boundary in South China and its effects on mass extinction. *Acta Geologica Sinica*, **63**, 169–180 (in Chinese with English abstract).

Yu J.X., Broutin J., Chen Z.Q., Shi X., Li H., Chu D.L. & Huang Q. (2015) Vegetation changeover across the Permian–Triassic Boundary in Southwest China: extinction, survival, recovery and palaeoclimate: a critical review. *Earth-Science Reviews*, **149**, 203–224.

Yusoff Z.M., Ngwenya B.T. & Parsons I. (2013) Mobility and fractionation of *REEs* during deep weathering of geochemically contrasting granites in a tropical setting, Malaysia. *Chemical Geology*, **349**, 71–86.

Zhang S.X., Yuan P., Zhao L.S., Tong J.N., Yang H., Yu J.S. & Shi Y.F. (2009) Clay rocks around Permian–Triassic boundary at Daxiakou section in Hubei Province, China. *Journal of Earth Science*, **20**, 909–920.

Zielinski R.A. (1985) Element mobility during alteration of silicic ash to kaolinite – a study of tonstein. *Sedimentology*, **32**, 567–579.

https://doi.org/10.1180/clm.2021.2 Published online by Cambridge University Press